Earthq Eng & Eng Vib (2021) 20: 727-745 **DOI**: https://doi.org/10.1007/s11803-021-2049-0

Reaching law based sliding mode control for a frame structure under seismic load

Ying Zhao[1†], Mohammad Noori[1‡,2§] and Wael A. Altabey[1,3*]

1. *International Institute for Urban Systems Engineering, Southeast University, Nanjing 210096, China*
2. *Department of Mechanical Engineering, California Polytechnic State University, San Luis Obispo, CA 93405, USA*
3. *Department of Mechanical Engineering, Faculty of Engineering, Alexandria University, Alexandria 21544, Egypt*

Abstract: Implementation of efficient vibration control schemes for seismically excited structures is becoming more and more important in recent years. In this study, the influence of different control schemes on the dynamic performance of a frame structure excited by El Centro wave, with an emphasis on reaching law based control strategies, is examined. Reaching law refers to the reachable problem and criteria for the sliding state of a control system. Three reaching laws are designed to present different sliding mode control strategies by incorporating a state space model that describes structural dynamic characteristics of a frame structure. Both intact and damaged structures are studied by using the aforementioned control strategies. The influence of different structural damage extents, control locations and reaching law based control methods are further investigated. The results show that the structure can be well controlled using the sliding mode strategy when the induced structural damage extent does not exceed the standard percentage for considering the structure was damaged, which is 20% reduction in structure stiffness, as reported in the literature. The control effectiveness is more satisfactory if the control location is the same as the direction of external excitation. Furthermore, to study the chattering phenomenon of the sliding mode control method, approximation and detail components extracted from the phase plots of the sliding mode control system are compared via wavelet transform at different scales. The results show that for the same type of control law, the system behaves with similar chattering phenomenon.

Keywords: reaching law; sliding mode control; state-space model; phase plot; 2-D wavelet transform

1 Introduction

Large and complex civil and mechanical structural systems need comprehensive management and maintenance over the entire life cycle, particularly various types of disasters happen. To cope with these challenges, development of efficient system identification and structural vibration control technologies has become an important issue (Zhao *et al*., 2018a; Narjabadifam *et al*., 2021; Ghannadi *et al*., 2020; Altabey *et al*., 2021; Altabey, 2017a). Since the introduction of variable structure control (VSC) or sliding mode control (SMC), these strategies have become some of the most popular approaches for vibration control of nonlinear systems (Slotine and Li, 1991), especially in the field of structural health monitoring and structural vibration control of systems such as buildings, bridges and wind turbines or in other practical applications (Mekki *et al.*, 2015; Grass *et al.*, 2008; Agrachev *et al.*, 2004; Hu *et al.*, 2017; Hušek, 2016; Yang *et al.*, 1997; De Leon-Morales, 2011; Altabey, 2016; Altabey, 2017b, 2017c, 2017d, 2017e; Altabey, 2018; Altabey and Noori, 2017; Altabey and Noori, 2018; Altabey *et al.*, 2020a, 2020b; Zhao *et al*., 2018b). Designing effective control laws can provide the desired performance to the closed-loop system in the presence of these disturbances/uncertainties (Liu and Wang, 2012; Shtessel *et al.*, 2014). The essential property of SMC is that the discontinuous feedback control switches on one or more manifolds are in the state space. Thus, the structure of the feedback system is altered or switched as the state crosses each discontinuous surface (Zinober, 1994). A survey of fundamental concepts and methodologies of sliding mode control have been carried out (Tokat *et al.*, 2015; Decarlo *et al.*, 1988; Hung *et al.*, 1993; Šabanovic, 2011; Bandyopadhyay *et al.*, 2013; Emel′Yanov *et al.*, 1996; Boiko, 2005).

SMC has a wide range of applications in structural health monitoring and vibration control. SMC was successfully utilized for controlling the vibration of tall

Correspondence to: Wael A. Altabey, International Institute for Urban Systems Engineering, Southeast University, Nanjing 210096, China; Department of Mechanical Engineering, Faculty of Engineering, Alexandria University, Alexandria 21544, Egypt
E-mail: wael.altabey@gmail.com
[†]Assistant Professor; [‡]Affiliate Professor; [§]Professor;
[*]Associate Professor
Received January 10, 2020; **Accepted** April 25, 2021

buildings with an active tuned mass damper (ATMD) installed at the top floor (Adhikari and Yamaguchi, 1997). It was also presented for seismic control of buildings isolated by a frictional-type sliding-isolation system (Yang *et al.*, 1996). This control strategy was also investigated for reducing the dynamic responses of building structures with hybrid base-isolation protective systems (Zhao *et al.*, 2000). A squeeze-mode electro-rheological (ER) mount was designed, manufactured, and applied to the vibration control of a frame structure subjected to external excitations (Hong *et al.*, 2002). A nonlinear single-degree-of-freedom structural system model excited by an earthquake was studied by modeling hysteresis and system nonlinearity (Baradaran-nia *et al.*, 2012). Based on genetic algorithms (GAs), a fuzzy sliding mode control (FSMC) method for the building structure was designed to ensure its safety and stability (Yu *et al.*, 1998; Wang and Lee, 2002). The FSMC method was also applied to seismic isolation of earthquake-excited structures (Alli and Yakut, 2005). A three-story shear building model subjected to ground excitations was considered by applying a RBF neural network to the switching surface (Li *et al.*, 2010). The response prediction of beam-like structures was studied via the deep learning based approach (Wang *et al.*, 2020a; Altabey, 2021, Kost *et al.*, 2019; Zhao *et al.*, 2018c). The performance and robustness of the SMC-based semi-active control system using MR dampers was investigated, and was effectively applied to a benchmark cable-stayed bridge (Moon *et al.*, 2003). An alternative design method of sliding mode control was proposed for practical implementation on nonlinear isolated bridges (Lee and Chen, 2011). An application of adaptive FSMC was presented for a benchmark problem on a seismically excited highway bridge (Ning *et al.*, 2009). A discrete time sliding mode controller using multi-rate output feedback was designed to minimize structural vibration of a cantilever beam using shape memory alloy wires as control actuators and piezo-ceramics as sensor and disturbance actuators (Kaliaperumal *et al.*, 2016). Control performances of a vehicle seat suspension system equipped with magneto-rheological dampers was studied using a new adaptive fuzzy sliding mode controller (Shin *et al.*, 2016). An attitude controller based on non-singular terminal sliding mode control was designed to effectively show damage and dynamic characteristics in an aircraft (Feng *et al.*, 2014).

Due to the characteristics of sliding mode control, the chattering effect is a critical problem. In the industrial field, chatter detection in the ball end milling process was proposed by monitoring dynamic cutting forces using wavelet transform (Tangjitsitcharoen *et al.*, 2015; Wang and Liang, 2009; Cao *et al.*, 2013; Yao *et al.*, 2010; Fu *et al.*, 2016). By using variational mode decomposition and wavelet packet decomposition, milling chatter based on energy entropy was studied (Zhang *et al.*, 2016). Chattering detection on ground cylindrical parts was also conducted by analyzing the time-frequency domain of the vibration signal via wavelet transform (González-Brambila *et al.*, 2006). Furthermore, wavelet analysis and multi-resolution analysis have been applied to singularity detection of mode shape and curvature mode of structures with some extent of damage (Zhao *et al.*, 2017, 2018d; Noori *et al.*, 2018; Wang *et al.*, 2020b, 2021; Li *et al.*, 2021).

On the other hand, an important group of methods for vibration control of structures under uncertainties, include robust control (Wang *et al.*, 2004; Huo *et al.*, 2016; Wang, 2003; Adeli *et al.*, 2004; Pourzeynali *et al.*, 2016), optimal control (Kim *et al.*, 2000), Neural Network based vibration control (Ghaboussi, 1995; Cho *et al.*, 2005; Blachowski and Pnevmatikos, 2018). Although considerable work has been done on the improvement of the robustness and reliability of sliding mode control algorithms, few researchers have studied the effect of structural damage on the effectiveness of control strategies, control location and chattering problem of different control laws. To the best of the authors′ knowledge, for the general chattering phenomenon in the sliding mode control, no effective tools have been developed to detect and compare different types of singularity similarity of signals. To investigate the impact of the chattering problem in obtaining law based control, 2-D wavelet decomposition and reconstruction are used to extract the approximation and detailed signal components of phase plots of the control system. It is proved to be a promising tool for singularity detection and feature extraction of 2-D images, which reveals the chattering phenomenon of the control system.

2 Control system modeling

2.1 State space model

Figure 1 shows a three degree-of-freedom (DOF) model of a building structure equipped with control actuators installed at different locations. The three control strategies, illustrated in this figure, include a base isolation, a bracing system and a tuned mass damper installed at various floor locations, where $\boldsymbol{u}$ denotes control input.

Figure 2 shows a schematic diagram of the reaching law based sliding mode control applied to the 3DOF structure using the MATLAB Simulink toolbox. The El Centro wave is the input signal of the system.

The control input $\boldsymbol{u}$, $\boldsymbol{e}$ is the tracking error vector of trajectory signals, and d$\boldsymbol{e}$ is the first order differential expression. Parameter $\boldsymbol{y}$ is a multi-dimensional vector that represents displacements and velocities of different floors of the structure. The vector equation of motion for the superstructure, for a more generalized model consisting of $n+1$ degrees of freedom, subjected to a one-dimensional earthquake ground motion, is given by:

$$\boldsymbol{M}\ddot{\boldsymbol{x}}(t)+\boldsymbol{C}\dot{\boldsymbol{x}}(t)+\boldsymbol{K}\boldsymbol{x}(t)=\boldsymbol{P}\boldsymbol{u}(t)+\boldsymbol{Q}\boldsymbol{w}(t) \tag{1}$$

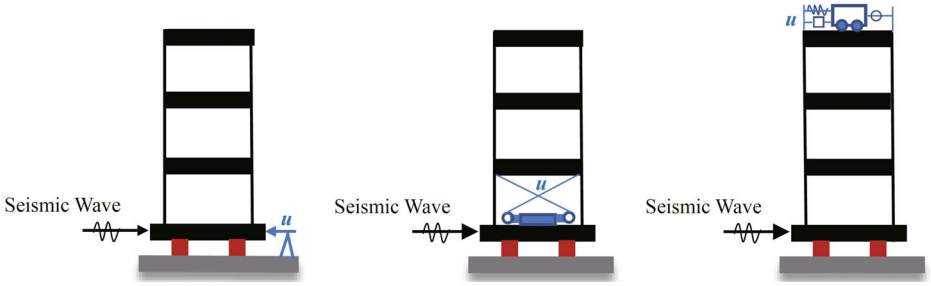

Fig. 1 Different strategies for structural control

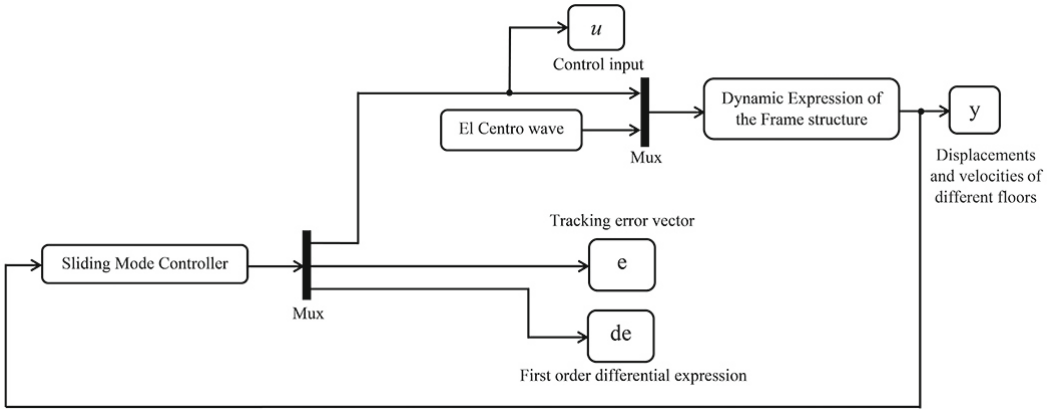

Fig. 2 Sliding mode control using reaching law

where $\boldsymbol{x}(t)=[x_n, x_{n-1}, \cdots, x_1, x_b]^{\mathrm{T}}$ is an $n+1$ order vector with x_i being the displacement of the ith story relative to the ground. Parameters $\boldsymbol{M}, \boldsymbol{C}, \boldsymbol{K}$ represent $(n+1)\times(n+1)$ mass, damping and stiffness matrices, respectively. Suppose that the primary structure of the building behaves linearly and is elastic. In other words, the stiffness coefficients $k_1, k_2, \cdots, k_n$ and damping coefficients $c_1, c_2, \cdots, c_n$ are supposed to be constants. In general, Eqs. (2) and (3), the time-dependent stiffness and damping coefficients $K_{\mathrm{t}}(t)$ and $K_{\mathrm{b}}(t)$, and $c_{\mathrm{t}}(t)$ and $c_{\mathrm{b}}(t)$ are introduced on the top and base floor, respectively, for the controlled system. These equations are related to the diagram representations in Fig. 2. For simplicity, these coefficients are assumed as constant herein. In Eq. (1), the structural stiffness and damping matrix are denoted as:

$$\boldsymbol{K}=\begin{bmatrix} k_{\mathrm{t}}(t)+k_n & -k_n & & & \\ -k_n & k_n+k_{n-1} & -k_{n-1} & 0 & \\ & \ddots & \ddots & \ddots & \\ 0 & -k_2 & k_2+k_1 & -k_1 & \\ & & -k_1 & k_1+k_{\mathrm{b}}(t) & \end{bmatrix} \tag{2}$$

$$\boldsymbol{C}=\begin{bmatrix} c_{\mathrm{t}}(t)+c_n & -c_n & & & \\ -c_n & c_n+c_{n-1} & -c_{n-1} & 0 & \\ & \ddots & \ddots & \ddots & \\ 0 & -c_2 & c_2+c_1 & -c_1 & \\ & & -c_1 & c_1+c_{\mathrm{b}}(t) & \end{bmatrix} \tag{3}$$

In Eq. (1), $\boldsymbol{P}$ is an $(n+1)\times m$ location matrix of the control force, $\boldsymbol{Q}$ is an $(n+1)\times s$ location matrix of the external loads, is a vector of the m control forces, and $\boldsymbol{u}(t)=[u_1, u_2, \cdots, u_m]^{\mathrm{T}}$ is a vector of the s external environmental loads or disturbances. Equation (1) can be converted into the state-space equation as shown in the following form:

$$\dot{\boldsymbol{z}}(t)=\boldsymbol{A}\boldsymbol{z}(t)+\boldsymbol{B}\boldsymbol{u}(t)+\boldsymbol{E}\boldsymbol{w}(t) \tag{4}$$

where $\boldsymbol{z}(t)=[z_1, z_2, \cdots, z_{2n+2}]^{\mathrm{T}}$ is a state vector of the order $(2n+2)$, $\boldsymbol{A}$ is a $(2n+2)\times(2n+2)$ system matrix, $\boldsymbol{B}$ is a $(2n+2)\times m$ control matrix and $\boldsymbol{E}$ is a $(2n+2)\times s$ disturbance matrix. The parameter $l=1$ because for each control case, there is assumed to be only one control force applied. They are expressed as follows.

$$\boldsymbol{z}(t)=\begin{bmatrix} \boldsymbol{x}(t) \\ \dot{\boldsymbol{x}}(t) \end{bmatrix} \tag{5}$$

$$\boldsymbol{A}=\begin{bmatrix} \boldsymbol{0} & \boldsymbol{I} \\ -\boldsymbol{M}^{-1}\boldsymbol{K} & -\boldsymbol{M}^{-1}\boldsymbol{C} \end{bmatrix} \tag{6}$$

$$\boldsymbol{B}=\begin{bmatrix} \boldsymbol{0} \\ \boldsymbol{M}^{-1}\boldsymbol{P} \end{bmatrix} \tag{7}$$

$$\boldsymbol{E}=\begin{bmatrix} \boldsymbol{0} \\ \boldsymbol{M}^{-1}\boldsymbol{Q} \end{bmatrix} \tag{8}$$

$$\boldsymbol{A}=\begin{bmatrix} 0 & 0 & 0 & 0 & 1 & 0 & 0 & 0 \\ 0 & 0 & 0 & 0 & 0 & 1 & 0 & 0 \\ 0 & 0 & 0 & 0 & 0 & 0 & 1 & 0 \\ 0 & 0 & 0 & 0 & 0 & 0 & 0 & 1 \\ -\dfrac{k_3+k_t}{m_3} & \dfrac{k_3}{m_3} & 0 & 0 & -\dfrac{c_3+c_t}{m_3} & \dfrac{c_3}{m_3} & 0 & 0 \\ \dfrac{k_3}{m_2} & -\dfrac{k_2+k_3}{m_2} & \dfrac{k_2}{m_2} & 0 & \dfrac{c_3}{m_2} & -\dfrac{c_2+c_3}{m_2} & \dfrac{c_2}{m_2} & 0 \\ 0 & \dfrac{k_2}{m_1} & -\dfrac{k_1+k_2}{m_1} & \dfrac{k_1}{m_1} & 0 & \dfrac{c_2}{m_1} & -\dfrac{c_1+c_2}{m_1} & \dfrac{c_1}{m_1} \\ 0 & 0 & \dfrac{k_1}{m_b} & -\dfrac{k_1+k_b}{m_b} & 0 & 0 & \dfrac{c_1}{m_b} & -\dfrac{c_1+c_b}{m_b} \end{bmatrix} \tag{9}$$

$$\boldsymbol{B}=\begin{bmatrix} 0 \\ 0 \\ 0 \\ 0 \\ 0 \\ 0 \\ 0 \\ \dfrac{1}{m_b} \end{bmatrix} \tag{10}$$

$$\boldsymbol{E}=\begin{bmatrix} 0 \\ 0 \\ 0 \\ 0 \\ 0 \\ 0 \\ 0 \\ \dfrac{1}{m_b} \end{bmatrix} \tag{11}$$

In the following section, parameter values are assigned as follows. The parameter $\boldsymbol{Q}$ indicates the base floor of the structure is directly excited by seismic wave.

$$m_3=m_2=m_1=m_b=1\ \text{kg} \tag{12}$$

$$k_3=k_2=k_1=100\frac{N}{m},\ k_t=k_b=50\frac{N}{m} \tag{13}$$

$$c_3=c_2=c_1=50\frac{Ns}{m},\ c_t=c_b=25\frac{Ns}{m} \tag{14}$$

$$\boldsymbol{Q}=\begin{bmatrix}0 & 0 & 0 & 1\end{bmatrix}^{\mathrm{T}} \tag{15}$$

2.1 Choice of location of control force *u*(*t*)

In general, when a seismic wave approaches a structure, the direct interaction between it and the upper structure is the base structure. However, if the building structure is relatively tall, the entire structural dynamic performance will be significantly influenced by both lateral wind load and seismic load, thus a damping and vibration control system should be considered in these locations. Therefore, reasonable design of the location of isolation system for a primary structure is a very challenging problem. Specifically, the choice of location of control input $\boldsymbol{u}(t)$ determines the effectiveness of the control strategy. The following cases represent the structural control locations where main damping and vibration control system is implemented. Correspondingly, location matrix vectors indicate the control force input.

(1) Base isolation system, where the building is mounted on a base-isolation platform supported by frictional bearings. In this case, $\boldsymbol{P}=\begin{bmatrix}0 & 0 & 0 & 1\end{bmatrix}^{\mathrm{T}}$.

(2) Active bracing system with actuators installed diagonally between the ground and first floor or other middle floors. In this case, $\boldsymbol{P}=\begin{bmatrix}0 & 0 & 1 & 0\end{bmatrix}^{\mathrm{T}}$ or $\begin{bmatrix}0 & 1 & 0 & 0\end{bmatrix}^{\mathrm{T}}$.

(3) Active tuned mass damper installed at the top floor. In this case, $\boldsymbol{P}=\begin{bmatrix}1 & 0 & 0 & 0\end{bmatrix}^{\mathrm{T}}$.

2.2 Choice of disturbance *w*(*t*)

In this study, in order to investigate and compare the effectiveness of the three control strategies described above, the structure is subjected to the El Centro earthquake wave as the external source of excitation. The El Centro wave is one of the most typical and common seismic waves selected for benchmark studies, and it has been widely used in modeling structural excitation and analyzing structural dynamic performance.

3 Design of sliding mode control

Consider the linear controllable system as:

$$\dot{\boldsymbol{z}}(t)=\boldsymbol{A}\boldsymbol{z}(t)+\boldsymbol{B}\boldsymbol{u}(t)+d(z,t) \tag{16}$$

where $d(z,t)$ is the disturbance term satisfying the constraint $d(z,t)\le\delta(z,t)$, and $\delta(z,t)$ is the upper bound of the disturbance. The control strategy is to find $\boldsymbol{u}$ such that $\boldsymbol{z}$ will track the desired trajectory $\boldsymbol{z}_{\mathrm{d}}$.

Let the tracking error vector be:

$$\boldsymbol{e}=\boldsymbol{z}-\boldsymbol{z}_{\mathrm{d}} \tag{17}$$

Herein, the goal of vibration suppression is to meet $\boldsymbol{z}_{\mathrm{d}}=0$ and then $\boldsymbol{e}=\boldsymbol{z}-0=\boldsymbol{z}$.

The design of sliding mode control involves two phases. The first phase is to select the switching hyper-plane $\boldsymbol{s}(\boldsymbol{e})$ to prescribe the desired dynamic characteristics of the controlled system. The second

phase is to design a controller to drive the state trajectory onto the sliding surface $\boldsymbol{s}(\boldsymbol{e})=\boldsymbol{s}(\boldsymbol{z})=0$ and make sure it remains there forever.

At the first stage, the m switching functions are chosen as:

$$\boldsymbol{s}(\boldsymbol{z})=\boldsymbol{R}\boldsymbol{z} \tag{18}$$

$$s_i(z)=r_i z=r_{i1}z_1+r_{i2}z_2+\cdots r_{i2n+2}z_{2n+2},\ i=1,2,\cdots,m \tag{19}$$

where $\boldsymbol{s}$ is a $m\times 1$ vector, $\boldsymbol{R}=\left[r_1,r_2,\cdots,r_m\right]^{\mathrm{T}}$ is a $m\times(2n+2)$ vector, and $\boldsymbol{r}_i=\left[r_{i1},r_{i2},\cdots,r_{i2n+2}\right]$, $\boldsymbol{r}_i$ is a sliding vector.

In the sliding mode, the system satisfies $\boldsymbol{s}(\boldsymbol{z})=0$ and $\dot{\boldsymbol{s}}(\boldsymbol{z})=0$, and through derivation, the control force is called the equivalent control force, i.e.,

$$\boldsymbol{u}_{\mathrm{eq}}=-(\boldsymbol{RB})^{-1}(\boldsymbol{RAz}+\boldsymbol{REw}) \tag{20}$$

Clearly, the control law of Eq. (20) cannot be synthesized explicitly if the external excitation term $d(z,t)$ is not known a priori, which is generally the case with the loading encountered in vibration problems related to such engineering structures. However, under appropriate conditions, the control given in Eq. (20) can be synthesized implicitly via discontinuous (chattering) control defined in terms of the known system parameters. Therefore, the term containing $d(z,t)$ is dropped from Eq. (20), and expressed as a term associated with ***Ew***, instead. This is achieved by a properly selected value of parameters η,g,α used in the design of control laws that impart a nonlinear switching discontinuous control action to account for the uncertainty in the excitation. The choice of η,g,α and hence, the control force $\boldsymbol{u}(t)$, must be such that the existence and the reachability of the sliding mode is guaranteed. Mathematically expressed, the condition that $\boldsymbol{s}^{\mathrm{T}}\cdot\dot{\boldsymbol{s}}<0$ must be satisfied. This results in:

$$\eta(t)\geq\left|(\boldsymbol{RB})^{-1}\boldsymbol{REw}\right| \tag{21}$$

The control law is chosen as follows:

$$\boldsymbol{u}=\boldsymbol{u}_{\mathrm{eq}}+\boldsymbol{u}_{\mathrm{h}} \tag{22}$$

The system exhibits invariance properties, yielding motion independent of certain parameter variations and disturbances. The equations governing the system dynamics may be obtained by substituting equivalent control denoted by $\boldsymbol{u}_{\mathrm{eq}}$ for the original control $\boldsymbol{u}$:

$$\boldsymbol{u}_{\mathrm{eq}}=-(\boldsymbol{RB})^{-1}\boldsymbol{RAz} \tag{23}$$

Parameter $\boldsymbol{u}_{\mathrm{eq}}$ is the equivalent control law that keeps the system states remaining on the sliding surface while $\boldsymbol{u}_{\mathrm{h}}$ is the hitting control law that drives the system states toward the sliding surface. Three different hitting control laws are described as follows:

Control Law 1: $$\boldsymbol{u}_{\mathrm{h}}=-(\boldsymbol{RB})^{-1}\eta\,\mathrm{sgn}(\boldsymbol{s})\quad\eta>0 \tag{24}$$

Control Law 2:

$$\boldsymbol{u}_{\mathrm{h}}=-(\boldsymbol{RB})^{-1}\left[\eta\,\mathrm{sgn}(\boldsymbol{s})+g\boldsymbol{s}\right]\quad\eta>0,k>0 \tag{25}$$

Control Law 3:

$$\boldsymbol{u}_{\mathrm{h}}=-(\boldsymbol{RB})^{-1}\eta|\boldsymbol{s}|^{\alpha}\,\mathrm{sgn}(\boldsymbol{s})\quad k>0,\alpha>0 \tag{26}$$

Different control laws indicate different reaching speed and ways towards the sliding plane. Control Law 1 is a constant rate reaching law. This reaching law constrains the switching variables to the sliding plane at a constant rate. Control Law 2 is an exponential reaching law. This reaching law forces the state to reach the sliding manifold in a faster way. Control Law 3 is a power rate reaching law. This reaching law increases the approaching speed when the state is far away from the sliding plane. A flowchart of the sliding mode controller procedures is presented in Fig. 3.

4 Continuous wavelet transform (CWT)

Continuous wavelet transform (CWT) is a convolution process of the data sequence with a set of continuous scaled and translated version of the mother

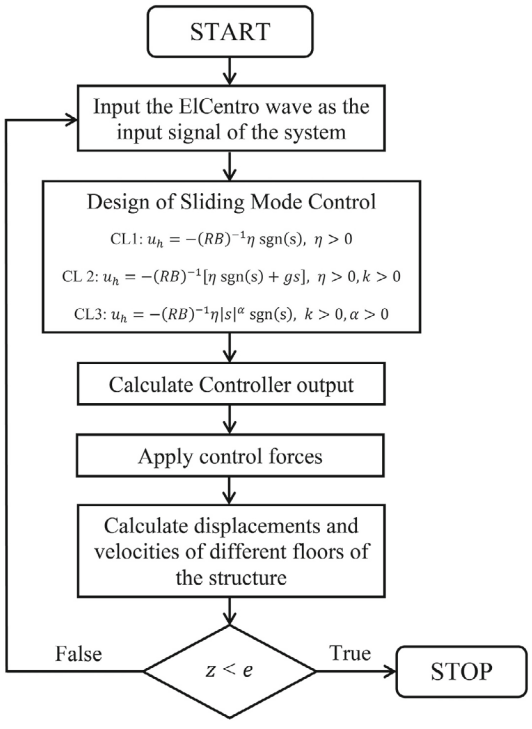

Fig. 3 Flow chart of the sliding mode controller procedures

wavelet (MW). The translating process is a smoothing effect over the length of the data sequence to localize the wavelet in the time domain, whereas the scaling process is compressing or the stretching of analyzed wavelet which indicates various resolutions. The stretched wavelet is used to capture the slow changes, while the compressed wavelet is used to capture abrupt changes in the signal. The trade-off of enhancing resolution is between increased computational cost and memory by computing wavelet components, and multiplying each component by the correctly dilated and translated wavelet, resulting in the constituent wavelet of the analyzed signal (Silik *et al.*, 2021a, 2021b, 2021c, 2021d; Kumar *et al.*, 2021; Ghiasi *et al.*, 2019, 2021).

4.1 2-D Continuous wavelet transform

In order to study the chattering phenomenon of the phase plane of the control system in a novel manner, a 2-D wavelet analysis is introduced for its superiority in singularity detection of image signals. The 2-D continuous wavelet transform (2-D CWT) is a representation of 2-D data in three determinant factors: position, dilation and rotation.

Position is a 2-D vector with real-valued elements, and dilation and rotation are real-valued scalars. Let $\boldsymbol{x}$ represents a vector with two real-valued elements.

$$\text{If} \quad f(x) \in L^2(\mathbb{R}^2) \tag{27}$$

is square-integrable on the plane, the 2-D CWT is defined as:

$$\begin{aligned} &\mathrm{WT}_{\mathrm{f}}(a,b,\theta) = \int_{\mathbb{R}^2} f(x) \frac{1}{a} \overline{\psi}\left(r_{-\theta}\left(\frac{x-b}{a} \right) \right) \mathrm{d}x \\ &a \in \mathbb{R}^+; x, b \in \mathbb{R}^2 \end{aligned} \tag{28}$$

where $\mathbb{R}$, $\mathbb{R}^+$ are real set and positive real set, respectively, ψ is the continuous wavelet function in the time domain, $\overline{\psi}$ is the conjugate function where the bar denotes the complex conjugate, and $\boldsymbol{r}_\theta$ is the 2-D rotation matrix:

$$\boldsymbol{r}_\theta = \begin{pmatrix} \cos(\theta) & -\sin(\theta) \\ \sin(\theta) & \cos(\theta) \end{pmatrix} \quad \theta \in [0, 2\pi) \tag{29}$$

The 2-D CWT is a space-scale representation of an image. For all the admissible 2-D wavelets, 2-D CWT can be regarded as a local filter for an image in scale and position. By applying 2-D wavelet transform, approximation and detail of signal components can be extracted at different scales or resolutions. It is an effective tool for feature extraction and edge detection of images. This property is later used for verification and comparison of the chattering phenomena of phase plots using different control laws developed for vibration control of the structure.

5 Response of intact and damaged structure with control

It is known from previous research reported in the literature that structures were considered to have damage when the stiffness for simulation of damage is down by 20% of its initial value, i.e., a 20% reduction in stiffness. By changing the structural stiffness coefficients, damage is considered to model the variation of structural characteristics. Figure 4 shows displacement and velocity response of the original intact structure excited by the El Centro seismic wave. The maximum displacements of the 3rd, 2nd, 1st and bottom floors of the intact structure are 0.0033 m, 0.0043 m, 0.0048 m and 0.0056 m, respectively, while the maximum velocity of the 3rd, 2nd, 1st and bottom floors of the intact structure are 0.0065 m/s, 0.0088 m/s, 0.0111 m/s and 0.0170 m/s, respectively.

Figure 5 shows displacement and velocity responses of the controlled original intact structure excited by the El Centro seismic wave. The maximum displacements

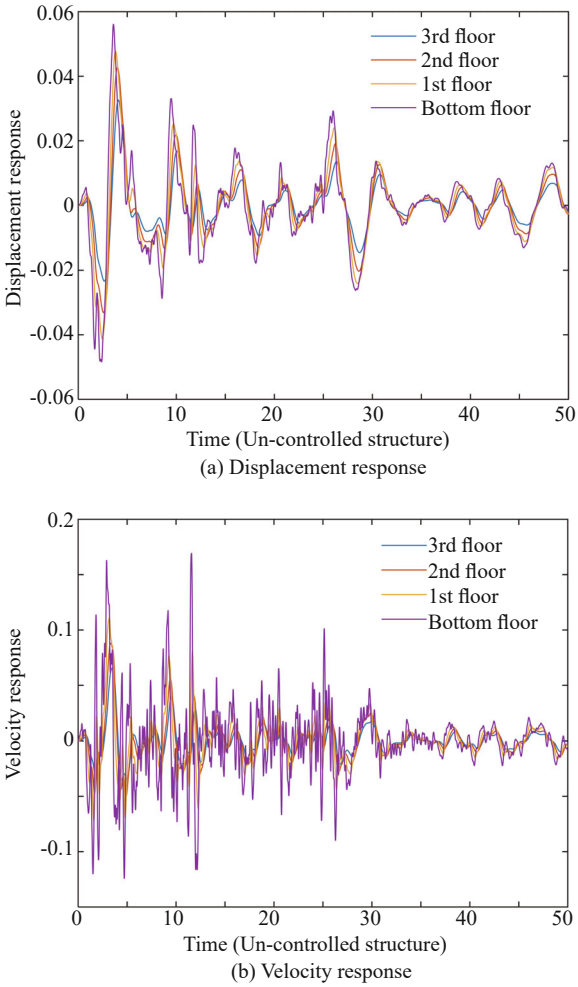

Fig. 4 Intact structure without control

of 3rd, 2nd, 1st and bottom floors of the intact structure are 0.0003 m, 0.0004 m, 0.0005 m and 0.0007 m, respectively, while the maximum velocity of 3rd, 2nd, 1st and bottom floors of the intact structure are 0.0004 m/s, 0.0006 m/s, 0.017 m/s and 0.0095 m/s, respectively. Herein, the control location is considered to be at the bottom of the structure, which is regarded as a base isolation system.

Figure 6 shows the control input $\boldsymbol{u}$ and phase plot of the system. The control input performs a relatively stable process, and the sliding trajectory indicates a relatively severe chattering phenomenon. The maximum chattering displacement reaches 0.0424 m. The corresponding control law is $\boldsymbol{u}_{\mathrm{h}} = -(\boldsymbol{RB})^{-1}\eta \mathrm{sgn}(\boldsymbol{s})$, where $\eta = 10$.

Based on the following cases, the maximum absolute values of displacement and velocity of the controlled structure excited by the El Centro seismic wave can be acquired.

(1) Control Law: control law 1 (CL1), control law 2 (CL2), control law 3 (CL3) as described above.

(2) Control Input Location: bottom floor, 1st floor, 2nd floor and 3rd floor.

(3) Damage Cases: 1st floor, 1st and 2nd floor, 1st, 2nd and 3rd floor (20% reduction of stiffness for simulation of damage).

The cases of the structure without control are shown in Table 1 and Table 2. As shown in Table 1 for the intact structure, damaged structure (1st floor), damaged structure (1st and 2nd floors) and damaged structure (1st, 2nd and 3rd floors), the maximum and minimum displacements occur at the bottom and 3rd floor, i.e., 0.056 m and 0.043 m, 0.058 m and 0.032 m, 0.058 m and 0.031 m, 0.058 m and 0.030 m, respectively. Compared with the intact structure, the displacement of the bottom structure increases by 3.57%, and the displacement of the bottom floor approximately decreases by 27.91%. As shown in Table 2, for the intact structure, damaged structure (1st floor), damaged structure (1st and 2nd floors) and damaged structure (1st, 2nd and 3rd floors), the maximum and minimum velocity occur at the bottom and 3rd floor, i.e., 0.170 m/s and 0.065 m/s, 0.171 m/s and 0.063 m/s, 0.171 m/s and 0.062 m/s, 0.171 m/s and 0.060 m/s, respectively. Compared with the intact structure, the velocity of the bottom structure increases by 3.57%, and the velocity of the 3rd floor approximately decreases by 4.62%.

The cases of the structure with control using three different control laws are shown in Figs. 7 and 8. The parameter values of the three control laws are $\eta = 10, g = 10, \alpha = 10$. As shown in Fig. 7, for the case

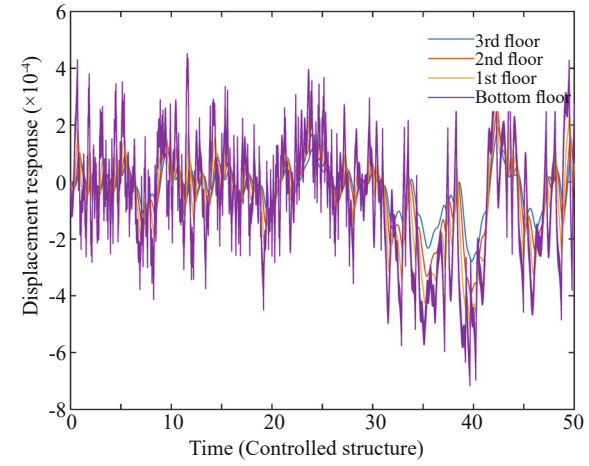

(a) Displacement response

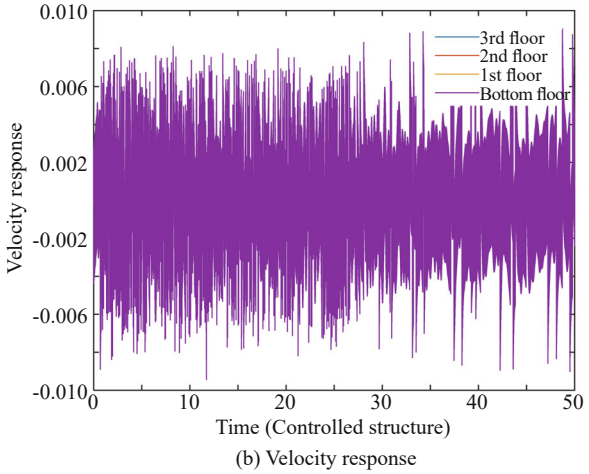

(b) Velocity response

Fig. 5 Intact structure with control

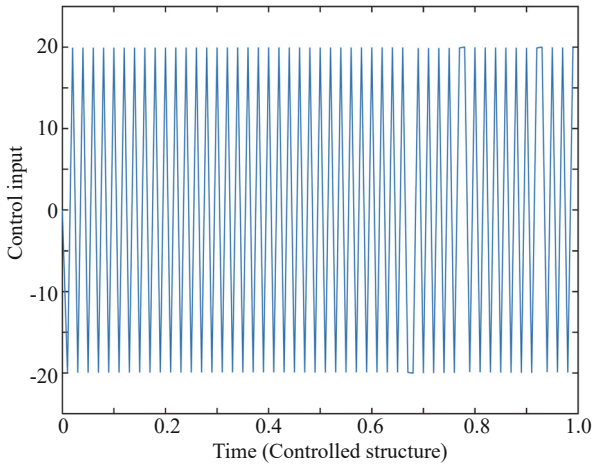

(a) Control input

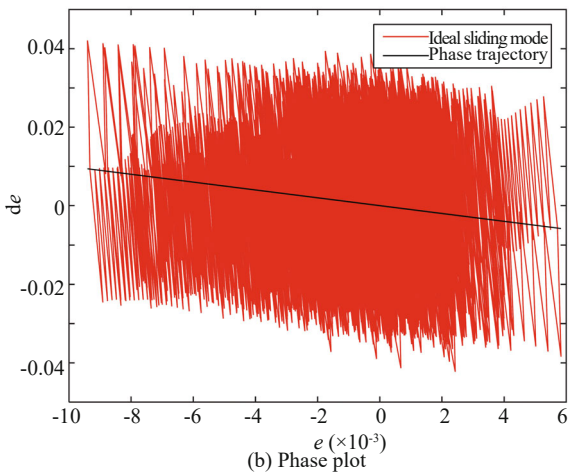

(b) Phase plot

Fig. 6 Sliding mode control

Table 1 Structure without control (displacement)

Displacement	Bottom floor	1st floor	2nd floor	3rd floor
Intact structure	0.056	0.048	0.043	0.043
Damaged structure (1st floor)	0.058	0.046	0.041	0.032
Damaged structure (1st and 2nd floors)	0.058	0.047	0.041	0.031
Damaged structure (1st, 2nd and 3rd floors)	0.058	0.047	0.041	0.030

Table 2 Structure without control (velocity)

Velocity	Bottom floor	1st floor	2nd floor	3rd floor
Intact structure	0.170	0.111	0.088	0.065
Damaged structure (1st floor)	0.171	0.108	0.086	0.063
Damaged structure (1st and 2nd floors)	0.171	0.110	0.083	0.062
Damaged structure (1st, 2nd and 3rd floors)	0.171	0.110	0.084	0.060

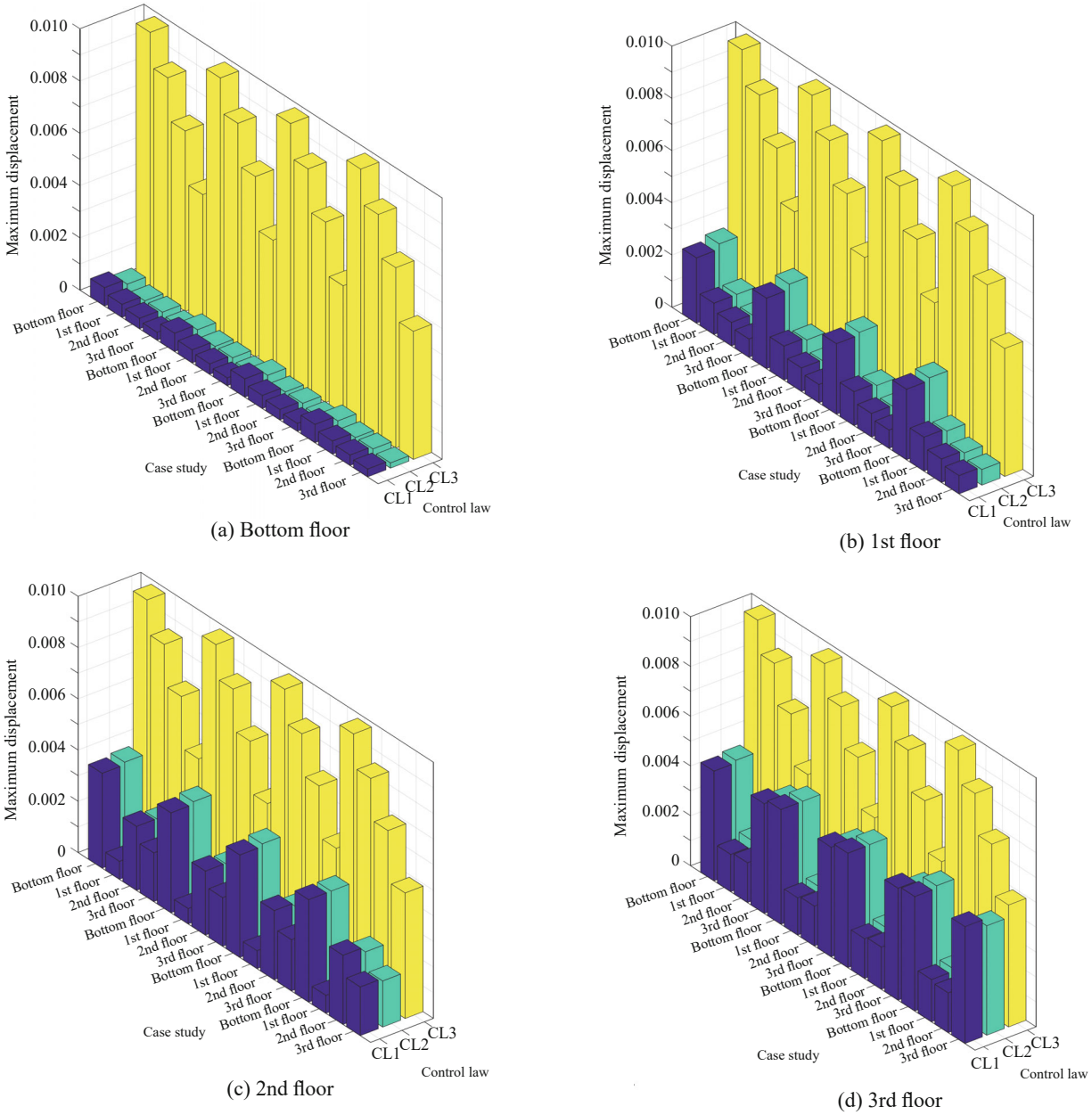

(a) Bottom floor (b) 1st floor

(c) 2nd floor (d) 3rd floor

Fig. 7 Maximum displacement (absolute value)

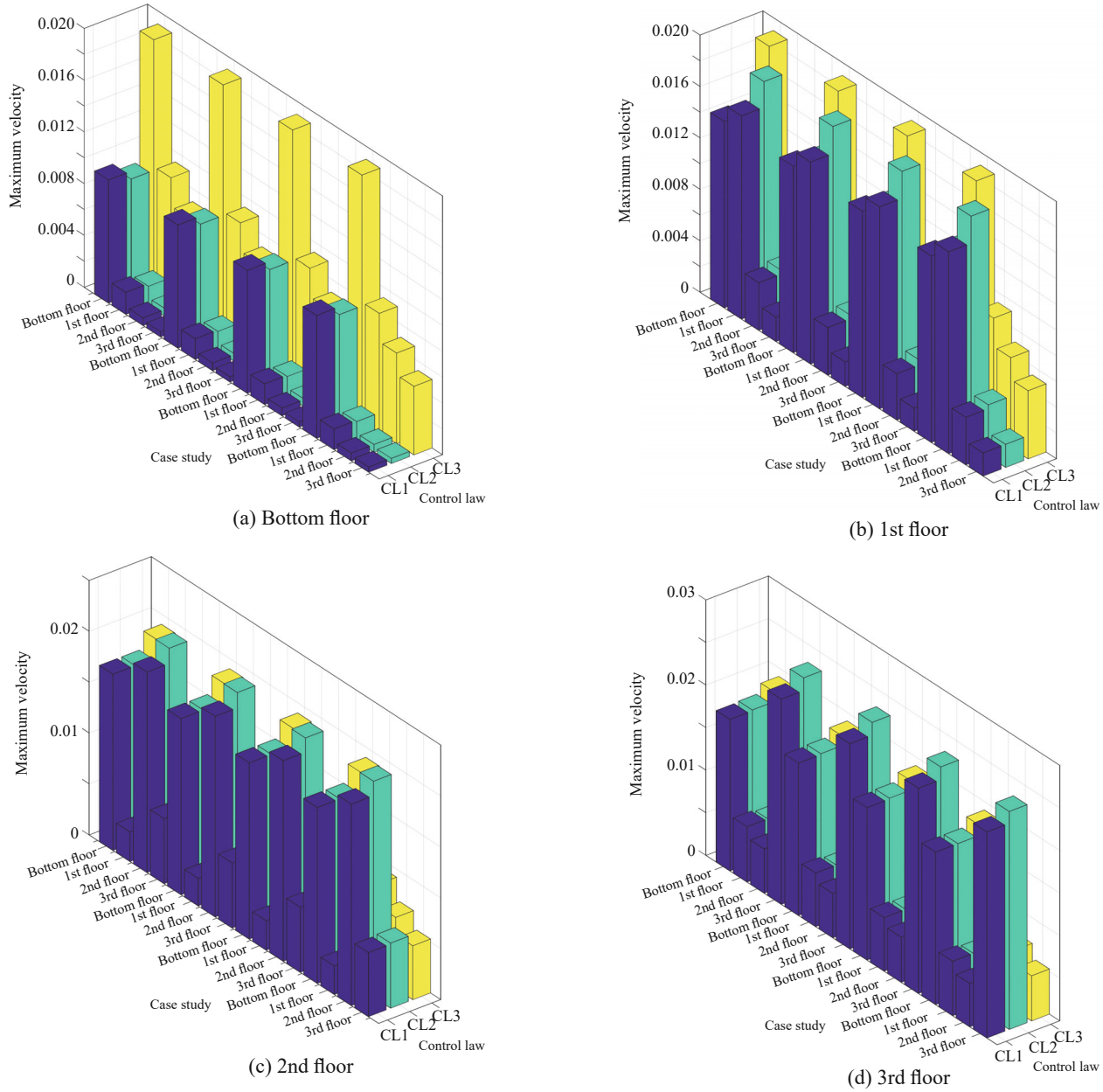

Fig. 8 Maximum velocity (absolute value)

when the control location is at the bottom floor using control law 1, control law 2 and control law 3 for the intact structure, damaged structure (1st floor), damaged structure (1st and 2nd floors) and damaged structure (1st, 2nd and 3rd floors), the maximum and minimum displacements occur at the bottom and 3rd floor, i.e., 0.0007 m and 0.0003 m, 0.0005 m and 0.0002 m, 0.0098 m and 0.0049 m, respectively. The maximum displacement first decreases by 28.57% (CL2-CL1), and then increases by 13 times (CL3-CL1). The minimum displacement first decreases by 33.3% (CL2-CL1), and then increases by 15.3 times (CL3-CL1). As shown in Fig. 8, for the case where the control location is at the bottom floor using control law 1, control law 2 and control law 3 for the intact structure, damaged structure (1st floor), damaged structure (1st and 2nd floors) and damaged structure (1st, 2nd and 3rd floors), the maximum and minimum velocity occurs at the bottom and 3rd floor, i.e., 0.0095 m/s and 0.0004 m/s, 0.0089 m/s and 0.0004 m/s, 0.0190 m/s and 0.0053 m/s, respectively. The maximum velocity first decreases by 6.32% (CL2-CL1), and then increases by 1 time (CL3-CL1). The minimum velocity first does not change (CL2-CL1), and then increases by 12.25 times (CL3-CL1). Figures 7 and 8 also show that for cases using the same control law and control location, the controlled structural displacement and velocity are almost the same, which means 20% damage in total may not affect the controlled maximum displacement and velocity of both the intact and damaged structure. Control law 1 has better control performance than control laws 2 and 3 since in this case, most of the maximum displacement

and velocity using control law 1 are smaller than control laws 2 and 3. Control location is also an influential factor that determines the control effect. If the control location is at the base floor, it shows better control effect on the structural dynamic performance.

6 Comparative study on chattering identification using different control strategies

In general, the phase plane generally describes the equilibrium status of a control system, and the sliding mode curve $s(z)=0$ describes the transient behavior of the system phase. Different control laws are developed to guarantee the existence of sliding motion and to maintain it in a finite time in the presence of uncertainty. According to the current position in the state space, the designed control law switches between different control structures to ensure the trajectories always move towards the switching condition, which is regarded as a variable structure control method. The ultimate trajectory is designed to slide within the boundaries of the control structures. The corresponding sliding motion consisting of geometrical locus and boundaries is called the sliding hyper surface. To design an SMC system, the first step is to construct a sliding plane, thus making the state variables of the plant dynamics restricted and constrained to a desired system response. Based on Lyapunov stability theory, the second step is designing switched feedback gains which drive the state trajectory of the plant to remain on the sliding surface.

The chattering phenomenon is described as a specific motion oscillating about the sliding manifold. Such a motion is mainly produced by two possible mechanisms. One mechanism is the lack of switching nonidealities such as delays, i.e., parasitic dynamics present in series with the plant, which causes a small amplitude oscillation with high frequency to appear within the neighborhood of the sliding manifold. These parasitic dynamics result from the stimulus of sensor dynamics and a fast actuator. The second mechanism is that the switching nonidealities alone can cause these high-frequency oscillations. The chattering phenomenon discussed herein is mainly caused by the second mechanism. To quantitively measure this phenomenon, a wavelet-based approach is introduced.

Figures 9 and 10 show the phase trajectory and ideal sliding mode when the system is designed with control law 2 and control law 3, respectively. As shown in these figures, for the case of control law 2, the chattering indicates considerable peaks while for the case of control law 3, the chattering indicates relatively smooth peaks. The sliding surface overall approximates the phase trajectory $s=0$. However, the direct implementation of the control laws results in the chattering problem, which is highly undesirable. Therefore, two-dimensional wavelet analysis of the *e*-d*e* plots is employed to show the signal detail variance. The parameter pairs assigned for the two different control laws are: $(\eta,g)=(1,1),(2,2),(3,3),(4,4),(5,5)$, and $(\eta,\alpha)=(1,1),(2,2),(3,3),(4,4),(5,5)$, respectively. The scale for the wavelet decomposition is chosen to change from 1 to 6.

The direct influence of chattering on the signal results in singularity of the signal. By applying the 2D wavelet transform of the *e*-d*e* plot using mother wavelet 'db5', both the approximation and detail signals reconstructed in the horizontal, vertical and diagonal directions are analyzed.

The approximation component refers to the low frequency part of the signal while the detail refers to the high frequency part of the signal. A 2-D rotation matrix shown in the 2-D wavelet transform theory determines the decomposition direction of the signal.

As shown in Figs. 11 and 12, parameters of the reaching law algorithms for CL2 and CL3 are assigned $(\eta,g)=(1,1)$ and $(\eta,\alpha)=(1,1)$, respectively, and the specific case using wavelet transform at scale 6 is presented herein.

Approximation wavelet coefficients represent the low frequency components of the signal depicted by the darkest parts, indicating relatively larger singularity, while the detail wavelet coefficients represent the high

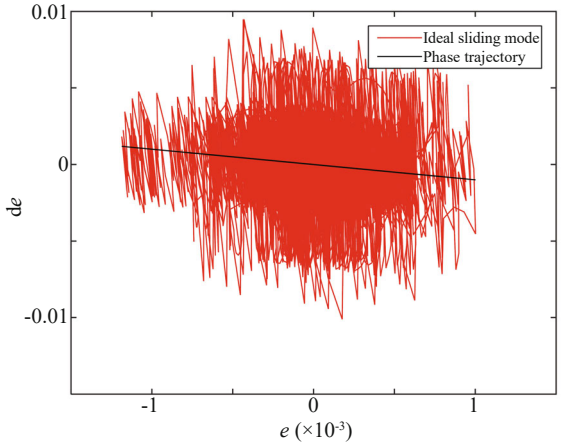

(a) CL2: $\eta=1$, $g=1$

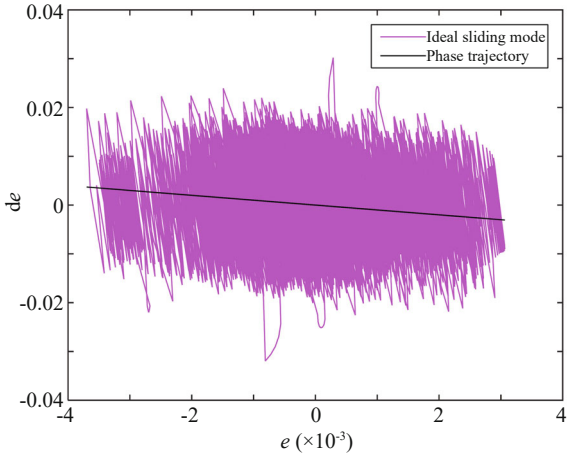

(b) CL2: $\eta=5$, $g=5$

Fig. 9 Phase plot

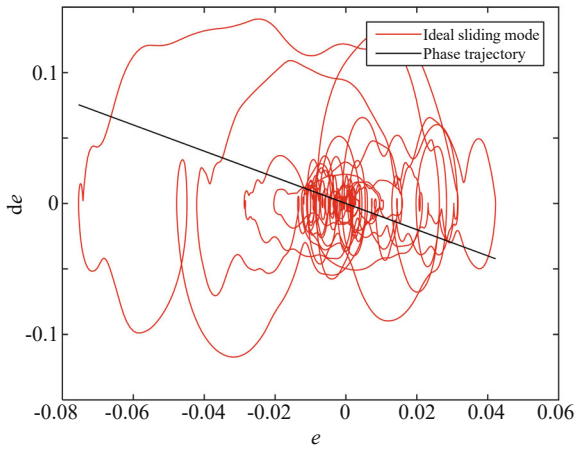

(a) CL3: $\eta = 1$, $\alpha = 1$

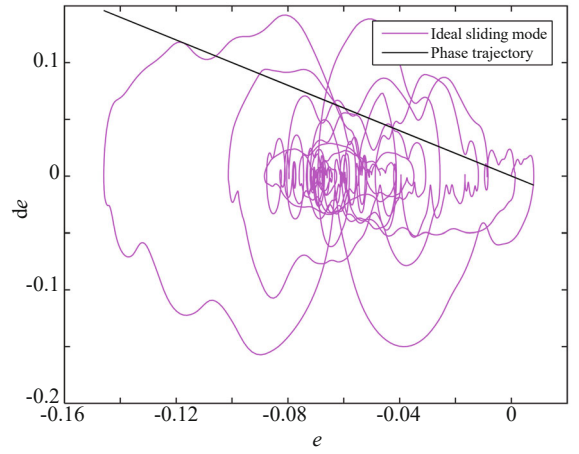

(b) CL3: $\eta = 5$, $\alpha = 5$

Fig. 10 Phase plot

frequency components depicted by the brightest parts, indicating relatively larger singularity. 2-D wavelet decomposition is realized by returning approximation and detail coefficients at different scales using decomposition low-pass and high-pass filters. The output wavelet 2-D decomposition structure $[\boldsymbol{C}, \boldsymbol{S}]$ contains the wavelet decomposition vector $\boldsymbol{C}$ and the corresponding bookkeeping matrix $\boldsymbol{S}$. Vector $\boldsymbol{C}$ is organized in Eq. (30):

$$\begin{aligned}\boldsymbol{C} = [&\boldsymbol{A}(N) \mid \boldsymbol{H}(N) \mid \boldsymbol{V}(N) \mid \boldsymbol{D}(N) \ldots \boldsymbol{H}(N-1) \\ &\mid \boldsymbol{V}(N-1) \mid \boldsymbol{D}(N-1) \ldots \boldsymbol{H}(1) \mid \boldsymbol{V}(1) \mid \boldsymbol{D}(1)]\end{aligned} \tag{30}$$

where $\boldsymbol{A}, \boldsymbol{H}, \boldsymbol{V}, \boldsymbol{D}$ are vectors representing approximation, horizontal detail, vertical detail and diagonal detail coefficients, respectively.

Table 3 and Table 4 quantitatively compare the similarity of phase plots of the control system implemented using CL 2 and CL3, respectively. As shown in Table 3, for different groups of parameters, the mean values of approximation coefficients of the *e*-d*e* plot for CL2 range from 218.2 to 227.1, 218.3 to 227.1, 247 to 247.7 for scale 2, 4, 6, respectively. The standard deviations range from 56.63 to 66.54 (increase by 19.6%), 53.44 to 64.73 (increase by 21.13%), 50.81 to 60.92 (increase by 19.9%) for scale 2, 4, 6, respectively. Similar cases are also applied for horizontal, vertical and diagonal wavelet detail coefficients. It can be seen that for the same scale, wavelet coefficients have similar values due to small deviations. These indicate that the change of the parameter pair (η, g) generally does not significantly affect the chattering phenomena for the

Table 3 Wavelet Decomposition (CL2)

Scale		Approximation coefficient		Detail coefficient					
				Horizontal direction		Vertical direction		Diagonal direction	
		M	S	M	S	M	S	M	S
(1,1)	2	227.1	57.33	0	8.739	0	13.97	0	2.800
	4	227.1	54.87	-0.02	4.629	0	9.2	0	2.642
	6	227.5	53.07	-0.298	5.757	0.052	5.638	0	2.285
(2,2)	2	225.0	56.63	0	9.031	0	16.55	0	3.554
	4	225.1	53.44	-0.025	4.980	0	10.28	0	3.100
	6	225.6	50.81	-0.325	7.029	0.163	6.826	0	3.222
(3,3)	2	224.0	59.90	0	9.059	0	15.03	0	3.457
	4	224.1	57.41	-0.027	5.220	0	8.803	0	2.903
	6	224.7	54.18	-0.198	7.807	0.138	7.076	0	2.346
(4,4)	2	218.2	66.54	0	8.686	0	14.25	0	3.104
	4	218.3	64.73	-0.026	4.712	0	7.59	0	3.030
	6	219.0	60.92	-0.253	10.50	0.161	4.505	0.004	2.848
(5,5)	2	221.8	65.22	0	8.730	0	12.87	0	3.031
	4	221.8	63.42	-0.026	4.977	0	6.904	0	3.064
	6	222.0	59.26	-0.215	9.874	0.057	8.643	0.002	3.514

Remark: M: mean, S: standard deviation, CL2 parameter assignment: (η, g)

Table 4 Wavelet decomposition (CL3)

Scale		Approximation coefficient		Detail coefficient					
				Horizontal direction		Vertical direction		Diagonal direction	
		M	S	M	S	M	S	M	S
(1,1)	2	246.3	21.33	0	9.636	0	11.29	0	4.768
	4	246.5	15.97	-0.02	5.258	0	6.366	0	3.433
	6	247.0	12.39	-0.235	5.433	0.078	4.664	0	2.519
(2,2)	2	247.0	20.73	0	9.459	0	11.22	0	4.679
	4	247.1	15.14	-0.02	5.318	0	6.549	0	3.121
	6	247.7	11.59	-0.323	4.213	0.098	5.726	0	1.911
(3,3)	2	246.7	20.62	0	9.679	0	11.06	0	4.872
	4	246.8	14.65	-0.02	5.281	0	6.500	0	3.374
	6	247.4	11.35	-0.279	4.711	0.11	4.411	0	1.762
(4,4)	2	246.6	20.46	0	9.652	0	11.14	0	4.902
	4	246.8	14.48	-0.02	5.384	0	6.436	0	3.489
	6	247.4	11.72	-0.279	4.733	0.104	3.053	0.002	1.811
(5,5)	2	246.6	20.55	0	9.662	0	11.15	0	4.899
	4	246.7	14.56	-0.02	5.392	0	6.421	0	3.399
	6	247.4	11.76	-0.278	4.778	0.104	3.062	0	1.819

Remark: M: mean, S: standard deviation, CL3 parameter assignment: (η, α)

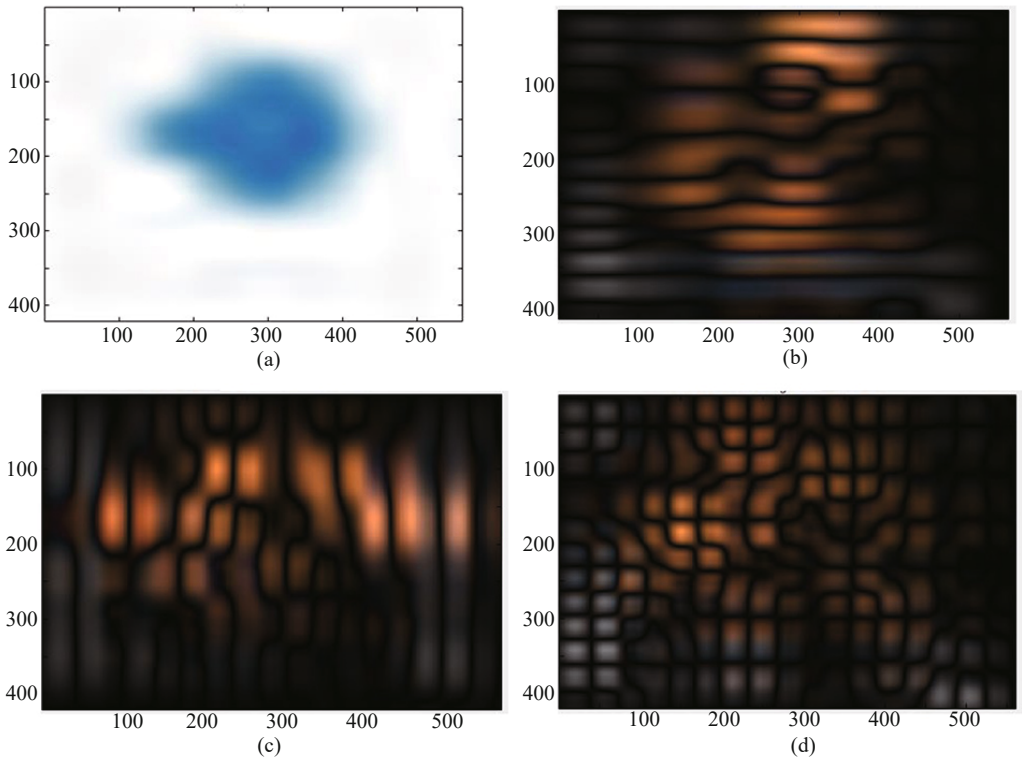

Fig. 11 Reconstructed signal at scale 6 (CL2), (a) approximation, (b) detail: horizontal direction, (c) detail: vertical direction and (d) detail: diagonal direction

same reaching law CL2.

As shown in Table 4, for different groups of parameters, the mean values of approximation coefficients of the *e*-d*e* plot for CL3 range from 246.3 to 247, 246.5 to 247.1, 247 to 247.7 for scale 2, 4, 6, respectively. The standard deviations range from 20.46 to 21.33 (increase by 4.25%), 14.48 to 15.97 (increase by 10.29%), 11.35 to 12.39 (increase by 9.16%) for scale 2, 4, 6, respectively. Similar cases are also applied for horizontal, vertical and diagonal wavelet detail coefficients. It can also be seen that for the same scale, wavelet coefficients have similar values due to

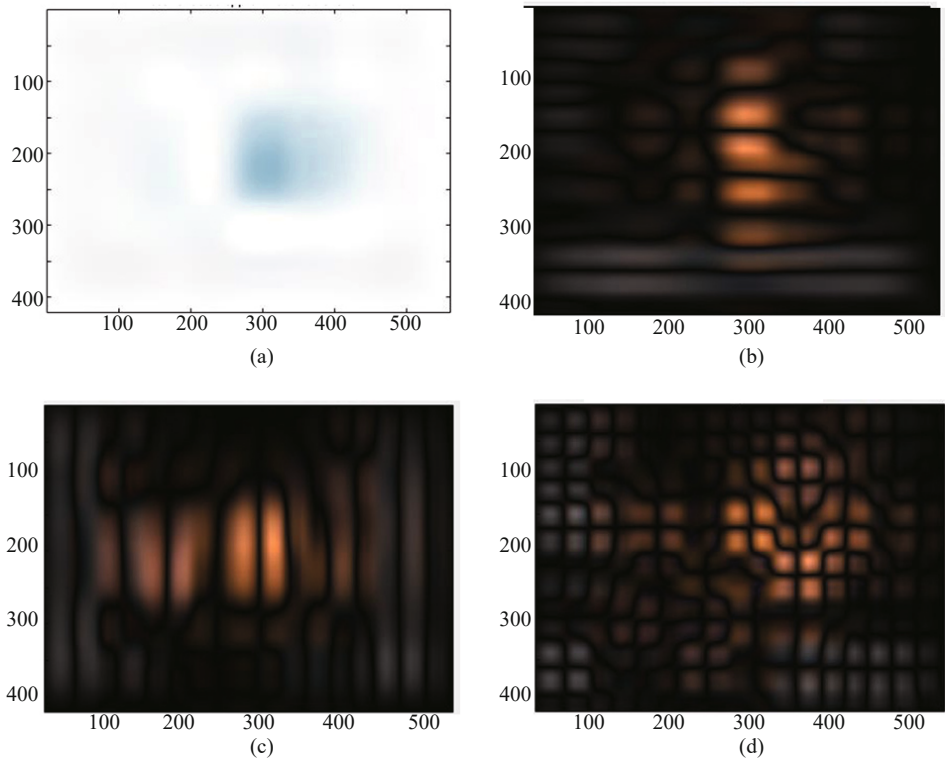

Fig. 12 Reconstructed signal at scale 6 (CL3), (a) approximation, (b) detail: horizontal direction, (c) detail: vertical direction and (d) detail: diagonal direction

small deviations. These deviations indicate the change of (η,α) generally does not significantly affect the chattering phenomena for the same reaching law CL3. However, the approximation wavelet coefficients for CL2 and CL3 have a relatively large difference, which demonstrates that different chattering effects are mainly influenced by the two different control strategies.

7 Discussion

In this section, the effect of structural damage, control location, and control law on the structural dynamic performance and chattering problem of different designed control systems are discussed by selecting several suitable cases to examine each of the effects to demonstrate the corresponding conclusions.

7.1 Effect of structural damage on structural control

Effective vibration control of structures under seismic load is important. However, if the structure is damaged, how to better design a control strategy becomes a critical issue. Here, three different case studies are selected to study this critical issue. The cases are: **Case 1:** Intact structure, control location is at the 1st floor, control law is CL1, **Case 2:** Damaged structure (1st floor), control location is at the 2nd floor, control law is CL3, and **Case 3:** Damaged structure (1st, 2nd and 3rd floor), control location is at the 3rd floor, control law is CL2.

Figure 13 presents a comparison of the maximum displacements and maximum velocity between the controlled and uncontrolled structure for the three different case studies. As shown in Fig. 13, the legend behind each plot in the figure represents the difference percentages between the controlled and uncontrolled structure for all the cases of control law. From the results, it can be seen that the absolute values of displacements and velocity of the controlled structure are 10 times smaller than the uncontrolled structure. In addition, from error analysis, it can be seen that in most cases, the structure has almost a 1 time reduction amplitude compared to the uncontrolled structure. Also, for the same location using the same control law, most of the absolute values of maximum displacement and velocity of the controlled structure are the same, for the case that the analyzed structures have a certain probability of damage (20% reduction of structural stiffness). The more significant observation, for case 2 and case 3 (damaged structure) compared with case 1 (intact structure), even when the control law and location change, the induced 20% damage does not significantly change the structural displacements and velocity (decrease by 50%–100%), which means that the structural performance will stay stable.

7.2 Effect of control location

Tall buildings are usually under lateral wind load, which has significant effect on structural integrity and comprehensive performance. Middle and top floors probability have large displacements and should be

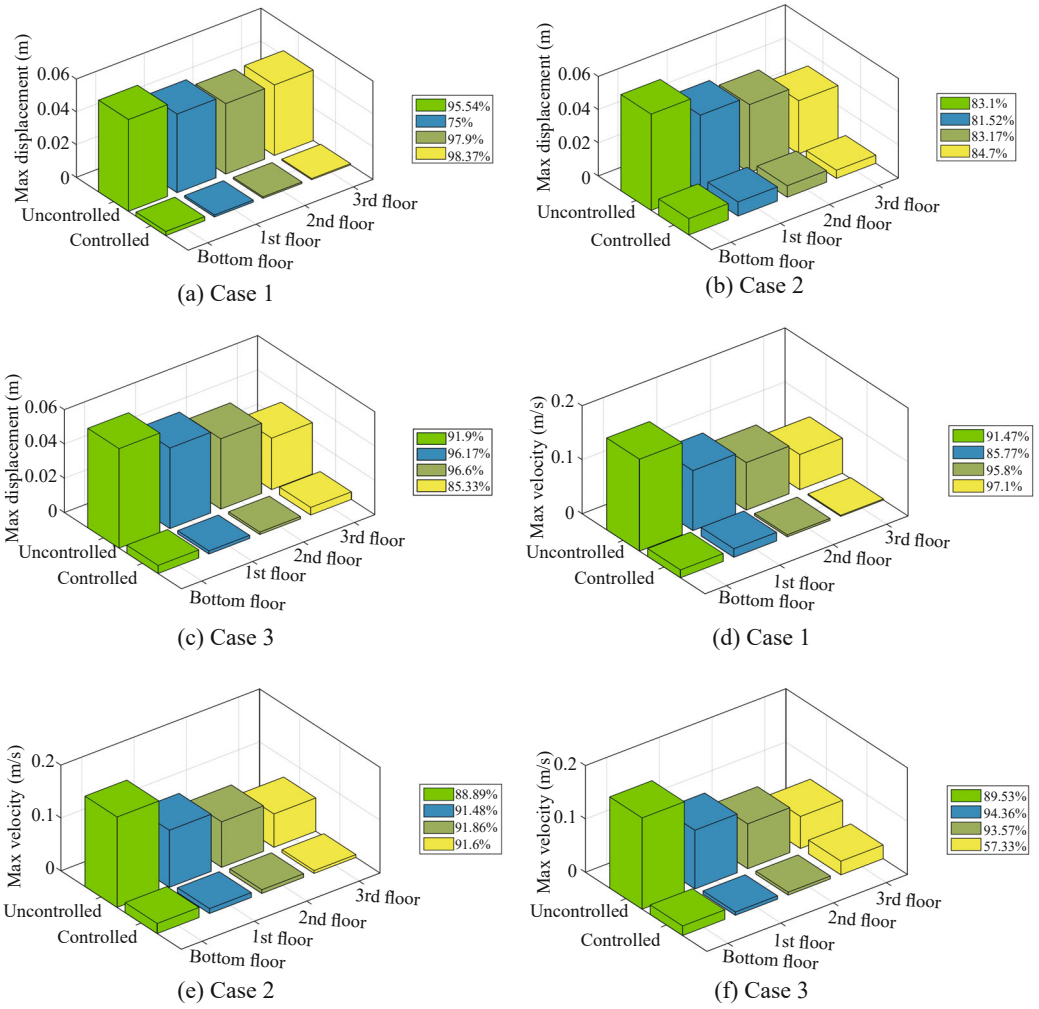

Fig. 13 A comparison of the maximum displacements and velocity between the controlled and uncontrolled structure

controlled effectively by installing dampers. Therefore, the effect of different control locations on structures is important. Here, three different case studies are selected to study this critical issue. The cases are: **Case 4:** Intact structure, control location is at the bottom, 1st, 2nd and 3rd floor, control law is CL1, **Case 5:** Damaged Structure (1st and 2nd floor), control location is at the bottom, 1st, 2nd and 3rd floor, control law is CL3, and **Case 6:** Damaged Structure (1st, 2nd and 3rd floor), control location is at the bottom, 1st, 2nd and 3rd floor, control law is CL2. For Case 4, the maximum structural displacements and velocities for bottom, 1st, 2nd and 3rd floors are 0.0007 m, 0.0025 m, 0.0037 m and 0.0044 m, respectively, and 0.0095 m/s, 0.0158 m/s, 0.0197 m/s, 0.0241 m/s, respectively for different control locations. It can be seen that the higher the control location is, the weaker structural vibration effectiveness performs. The control location at the bottom floor is better or more effective in suppressing the structural response than the 1st, 2nd and 3rd floor. Generally, the structure is subjected to a base excited seismic wave. In other words, if the control location is at the same location where external excitation exists, the control effect shows more satisfactory results for both intact and damaged structures. For case 5 and 6, similar conclusions can be drawn when implementing different control strategies.

7.3 Effect of different control strategies

Development of the reaching law based control algorithms is important for effective structural vibration control. The robustness of the control algorithm / control law has a direct effect on the controlled structure. CL1 is a constant rate reaching law, CL2 is an exponential reaching law, and CL3 is a power rate reaching law. For CL1, if the parameter η is small, the reaching time will be relatively long, while if it is too large, it will cause severe chattering. For CL2, the exponential term gs causes the state forced to switching manifold faster as s is large. For CL3, the reaching law causes the approaching speed to increase since the state is far away from the switching manifold. The reaching mode behaves as a fast and low chattering phenomenon.

Figures 9 and 10 show different sliding modes for different control laws. Table 3 and Table 4 show the effect of parameter change using CL2

$\boldsymbol{u}_{\mathrm{h}} = -(\boldsymbol{RB})^{-1}\left[\eta \operatorname{sgn}(\boldsymbol{s}) + g\boldsymbol{s}\right]$, where $(\eta, g) = (1,1)$ to $(5,5)$ and CL3 $\boldsymbol{u}_{\mathrm{h}} = -(\boldsymbol{RB})^{-1}\eta|\boldsymbol{s}|^{\alpha}\operatorname{sgn}(\boldsymbol{s})$, where $(\eta, \alpha) = (1,1)$ to $(5,5)$ on the intact structure with control. The results show that different control strategies behave differently from the sliding modes; however, they all move towards the phase trajectory where $s = 0$. 2-D wavelet transform shows the variance of wavelet coefficients (high frequency component as detail and low frequency component as approximation) does not change much for the same signal scale by using the same control law. However, the approximation coefficients of phase plots for different control laws have a relatively large difference. This means that the variance of parameters of the same control law have similar control robustness, and that the chattering phenomenon resulting from the same control law is similar.

8 Concluding remarks

In this study, a sliding mode control strategy based on different reaching laws is proposed to suppress the vibration of a three-story frame structure excited by a seismic wave. At the first step, a state space model was constructed based on the structural dynamic expression of a structure. Then, three control methods using constant, exponential and power reaching laws were employed to establish a sliding mode control system model. Different structural damage cases, control locations and control laws were investigated to demonstrate their influence on the structure. The results presented herein indicate that the incorporation of 20% structural damage has little effect on structural control effectiveness. It is more reasonable if the control location is at the bottom of the structure where the external seismic excitation is exerted. 2-D wavelet transform is used for feature extraction of the chattering phenomenon that exists in the phase plane of the sliding mode control system based on different control laws. By multiresolution analysis of decomposed images of phase plots, it is proved that as the control parameters change within a range, different control laws have a different influence on the control system based on different control laws.

Declaration of conflicting interests

The author(s) declare no potential conflicts of interest with respect to the research, authorship, and/or publication of this article.

Acknowledgement

Participation of the third author and the research study reported herein was made possible with funding from the Donald E. Bently Center for Engineering Innovation, Mechanical Engineering, Cal Poly, San Luis Obispo. In addition, the third author acknowledges the support provided as a distinguished visiting professor by Southeast University and the International Institute for Urban Systems Engineering.

References

Adhikari R and Yamaguchi H (1997) "Sliding Mode Control of Buildings with ATMD," *Earthquake Engineering and Structural Dynamics*, **26**(4): 409–422.

Agrachev AA, Morse AS, Sontag DE, Sussmann HJ, Utkin VI (2004), "Nonlinear and Optimal Control Theory," Springer, Berlin, Heidelberg. https://doi.org/10.1007/978-3-540-77653-6

Alli H and Yakut O (2005) "Fuzzy Sliding-Mode Control of Structures," *Engineering Structures*, **27**(2): 277–284. https://doi.org/10.1016/j.engstruct.2004.10.007

Adeli H, ASCE F and Kim H (2004), "Wavelet-Hybrid Feedback-Least Mean Square Algorithm for Robust Control of Structures," *Structural Engineering*, **130**(1): 128–137. https://doi.org/10.1061/(ASCE)0733-9445(2004)130:1(128)

Altabey WA (2016), "FE and ANN Model of ECS to Simulate the Pipelines Suffer from Internal Corrosion," *Structural Monitoring and Maintenance*, **3**(3): 297–314, http://dx.doi.org/10.12989/smm.2016.3.3.297

Altabey WA (2017a) "An Exact Solution for Mechanical Behavior of BFRP Nano-Thin Films Embedded in NEMS," *Advances in Nano Research*, **5**(7): 337–358. http://dx.doi.org/10.12989/anr.2017.5.4.337

Altabey WA (2017b), "Free Vibration of Basalt Fiber Reinforced Polymer (FRP) Laminated Variable Thickness Plates with Intermediate Elastic Support Using Finite Strip Transition Matrix (FSTM) Method," *Vibroengineering*, **19**(4): 2873–2885. http://dx.doi.org/10.21595/jve.2017.18154

Altabey WA (2017c), "Prediction of Natural Frequency of Basalt Fiber Reinforced Polymer (FRP) Laminated Variable Thickness Plates with Intermediate Elastic Support Using Artificial Neural Networks (ANNs) method," *Vibroengineering*, **19**(5): 3668–3678. http://dx.doi.org/10.21595/jve.2017.18209

Altabey WA (2017d), "Delamination Evaluation on Basalt FRP Composite Pipe by Electrical Potential Change," *Advances in Aircraft and Spacecraft Science*, **4**(5): 515–528. http://dx.doi.org/10.12989/aas.2017.4.5.515

Altabey WA (2017e), "EPC Method for Delamination Assessment of Basalt FRP Pipe: Electrodes Number Effect," *Structural Monitoring and Maintenance*, **4**(1): 69–84. http://dx.doi.org/10.12989/smm.2017.4.1.069

Altabey WA and Noori M (2017), "Detection of Fatigue Crack in Basalt FRP Laminate Composite Pipe Using Electrical Potential Change Method," *Phys.: Conf. Ser.*, **842**: 012079. http://dx.doi.org/10.1088/1742-6596/842/1/012079

Altabey WA and Noori M (2018), "Monitoring the Water Absorption in GFRE Pipes via an Electrical Capacitance sensors," *Advances in Aircraft and Spacecraft Science*, **5**(4): 411–434. http://dx.doi.org/10.12989/aas.2018.5.4.499

Altabey WA (2018), "High Performance Estimations of Natural Frequency of Basalt FRP Laminated Plates with Intermediate Elastic Support Using Response Surfaces Method," *Vibroengineering*, **20**(2): 1099–1107. http://dx.doi.org/10.21595/jve.2017.18456

Altabey WA, Noori M, Alarjani A and Zhao Y (2020a), "Tensile Creep Monitoring of Basalt Fiber-Reinforced Polymer Plates via Electrical Potential Change and Artificial Neural Network," *Scientia Iranica, International Journal of Science and Technology, Transactions on Mechanical Engineering* (*B*), **27**(4): 1995-2008. http://dx.doi.org/10.24200/SCI.2020.52754.2874

Altabey WA, Noori M, Alarjani A and Zhao Y (2020b), "Nano-Delamination Monitoring of BFRP Nano-Pipes of Electrical Potential Change with ANNs," *Advances in Nano Research*, **9**(1): 1–13. https://doi.org/10.12989/anr.2020.9.1.001

Altabey WA, Noori M, Wang T, Ghiasi R, Kuok SC and Wu Z (2021), "Deep Learning-Based Crack Identification for Steel Pipelines by Extracting Features from the 3D Shadow Modeling," *Applied Sciences*. https://www.mdpi.com/journal/applsci (in Press)

Altabey WA (2021), "Applying Deep Learning and Wavelet Transform for Predicting the Vibration Behavior in Variable Thickness Skew Composite Plates with Intermediate Elastic Support," *Vibroengineering*. https://doi.org/10.21595/jve.2020.21480 (in Press)

Bandyopadhyay B, Janardhanan S and Spurgeon SK (2013), "Advances in Sliding Mode Control," *Lecture Notes in Control and Information Sciences*, Springer, Berlin, Heidelberg, 21–53. https://doi.org/10.1007/978-3-642-36986-5

Boiko I (2005), "Analysis of Sliding Modes in the Frequency Domain," *International Journal of Control*, **78**(13): 969–981. https://doi.org/10.1007/978-0-8176-4753-7_4

Baradaran-nia M, Alizadeh G, Khanmohammadi S and Azar BF (2012) "Optimal Sliding Mode Control of Single Degree-of-Freedom Hysteretic Structural System," *Communications in Nonlinear Science and Numerical Simulation*, **17**(11): 4455–4466. https://doi.org/10.1016/j.cnsns.2012.01.008

Blachowski B and Pnevmatikos N (2018) "Neural Network Based Vibration Control of Seismically Excited Civil Structures," *Periodica Polytechnica Civil Engineering*, **62**(3): 620–628. https://doi.org/10.3311/PPci.11601

Cao H C, Lei Y and He Z (2013) "Chatter Identification in End Milling Process Using Wavelet Packets and Hilbert–Huang Transform," *International Journal of Machine Tools and Manufacture*, **69**: 11–19. https://doi.org/10.1016/j.ijmachtools.2013.02.007

Cho HC, Fadali MS, Saiid M and Lee KS (2005), "Neural Network Active Control of Structures with Earthquake Excitation," *International Journal of Control, Automation, and Systems*, **3**(2): 202–210. https://doi.org/10.1007/s11709-019-0544-4

Decarlo RA, Zak SH and Matthews GP (1988), "Variable Structure Control of Nonlinear Multivariable Systems: a Tutorial," *Proceedings of the IEEE*, **76**(3): 212–232. https://doi.org/10.1109/5.4400

De Leon-Morales J (2011), "Sliding Mode Controllers and Observers for Electromechanical Systems," Springer, Berlin, Heidelberg, 493–516. https://doi.org/10.1007/978-3-642-22164-4_18

Emel′Yanov SV, Korovin SK and Levant A (1996), "High-Order Sliding Modes in Control Systems," *Computational Mathematics and Modeling*, **7**(3): 294–318. https://doi.org/10.1007/BF01128162

Feng Y, Yu X and Man Z (2014), "Non-Singular Terminal Sliding Mode Control for Structural Damaged Aircraft," *In Proceedings IEEE Chinese Guidance*, Navigation and Control Conference, IEEE: 641–645. https://doi.org/10.1016/S0005-1098(02)00147-4

Fu Y, Zhang Y, Zhou H, Li D, Liu H, Qiao H and Wanga X (2016) "Timely Online Chatter Detection in End Milling Process," *Mechanical Systems and Signal Processing*, **75**: 668–688. https://doi.org/10.1016/j.ymssp.2016.01.003

Ghaboussi J (1995) "Active Control of Structures Using Neural Networks," *Engineering Mechanics*, **121**(4): 555–567. https://doi.org/10.1061/(ASCE)0733-9399(1995)121:4(555) 67

Ghannadi P, Kourehli SS, Noori M, Altabey W A (2020), "Efficiency of Grey Wolf Optimization Algorithm for Damage Detection of Skeletal Structures via Expanded Mode Shapes," *Advances in Structural Engineering*, **23**(13): 2850–2865. https://doi.org/10.1177/1369433220921000

Ghiasi R, Ghasemi MR, Noori M and Altabey WA (2019), "A Non-Parametric Approach Toward Structural Health Monitoring for Processing Big Data Collected from the Sensor Network, *Structural Health Monitoring 2019*: *Enabling Intelligent Life-Cycle Health Management for Industry Internet of Things (IIOT) - Proceedings of the 12th International Workshop on Structural Health Monitoring* (*IWSHM 2019*), September 10-12, Stanford, California, USA. http://dx.doi.org/10.12783/shm2019/32395

Ghiasi R, Noori M, Altabey W A, Silik A, Wang T and Wu Z (2021), "Uncertainty Handling in Structural Damage Detection via Non-Probabilistic Meta-Models and Interval Mathematics, a Data-Analytics Approach," *Applied Sciences,* **11**(2): 770. https://doi.org/10.3390/app11020770

Grass D, Caulkins JP, Feichtinger G, Tragler G and Behrens DA (2008) "Optimal Control of Nonlinear Processes," Springer, Berlin, Heidelberg. https://doi.org/10.1007/978-3-540-77647-5

González-Brambila O, Rubio E, Jáuregui JC and Herrera-Ruiz G (2006), "Chattering Detection in Cylindrical Grinding Processes Using the Wavelet Transform," *International Journal of Machine Tools and Manufacture*, **46**(15): 1934–1938. https://doi.org/10.1016/j.ijmachtools.2006.01.021

Hu Y, Chen MZQ and Li C (2017), "Active Structural Control for Load Mitigation of Wind Turbines via Adaptive Sliding-Mode Approach," *Franklin Institute*, **354**(11): 4311–4330. https://doi.org/10.1016/j.jfranklin.2017.04.002

Hung JY, Gao W and Hung JC (1993), "Variable Structure Control: A Survey," *IEEE Transactions on Industrial Electronics*, **40**(1): 2–22. https://doi.org/10.1109/41.184817.

Hong SR, Choi SB and Han MS (2002), "Vibration Control of a Frame Structure Using Electro-Rheological Fluid Mounts," *International Journal of Mechanical Sciences*, **44**(10): 2027–2045. https://doi.org/10.1016/S0020-7403(02)00172-8

Huo L, Qu C and Li H (2016), "Robust Control of Civil Structures with Parametric Uncertainties Through D-K Iteration," *The Structural Design of Tall and Special Buildings*, **25**: 158–176. https://doi.org/10.1002/tal.1233

Hušek P (2016) "Adaptive Sliding Mode Control with Moving Sliding Surface," *Applied Soft Computing*, **42**: 178–183. https://doi.org/10.1016/j.asoc.2016.01.009

Kost A, Altabey WA, Noori M and Awad T (2019), "Applying Neural Networks for Tire Pressure Monitoring Systems," *Structural Durability and Health Monitoring*, **13**(3): 247–266. http://dx.doi.org/10.32604/sdhm.2019.07025

Kaliaperumal D, Mangalanathan U and Deenadayalan E (2016), "Shape Memory Alloy Actuated Structural Control with Discrete Time Sliding Mode Control Using Multirate Output Feedback," *Vibration and Control*, **22**(5): 1338–1357. https://doi.org/10.1177/1077546314536916

Kim JT, Jung HJ and Lee IW (2000), "Optimal Structural Control Using Neural Networks," *Engineering Mechanics*, **126**(2): 201–205. https://doi.org/10.1061/(ASCE)0733-9399(2000)126:2(201)

Kumar R, Ismail M, Zhao W, Noori M, Yadav A R, Chen S, Singh V, Altabey W A, Silik A I H, Kumar G, Kumar J and Balodi A (2021), "Damage Detection of Wind Turbine System Based on Signal Processing Approach: A Critical Review," *Clean Techn Environ Policy*, **23**(2): 561–580. https://doi.org/10.1007/s10098-020-02003-w

Li Z, Noori M, Zhao Y, Wan C, Feng D and Altabey WA (2021) "A Multi-Objective Optimization Algorithm for Bouc-Wen-Baber-Noori Model to Identify Reinforced Concrete Columns Failing in Different Modes," *Proceedings of the Institution of Mechanical Engineers, Part L: Journal of Materials: Design and Applications*. https://doi.org/10.1177/14644207211020028 (in Press)

Lee TY and Chen PC (2011), "Sliding Mode Control for Nonlinear Isolated Bridges," *Earthquake Engineering*, **15**(4): 582–600. https://doi.org/10.1080/13632469.2010.526751

Liu J and Wang X (2012), "Advanced Sliding Mode Control for Mechanical Systems," Springer, Berlin, Heidelberg. https://doi.org/10.1007/978-3-642-20907-9

Li Z, Deng Z and Gu Z (2010), "New Sliding Mode Control of Building Structure Using RBF Neural Networks," *Chinese Control and Decision Conference*, IEEE: 2820–2825. https://doi.org/10.1109/CCDC.2010.5498707

Mekki H, Boukhetala D and Azar AT (2015), "Sliding Modes for Fault Tolerant Control," *Advances and Applications in Sliding Mode Control Systems*, Studies in Computational Intelligence. Springer: Cham, 407–433. https://doi.org/10.1007/978-3-319-11173-5_15

Moon SJ, Bergman LA and Voulgaris PG (2003), "Sliding Mode Control of Cable-Stayed Bridge Subjected to Seismic Excitation," *Engineering Mechanics*, **129**(1): 71–78. https://doi.org/10.1061/(ASCE)0733-9399(2003)**129**:1(71)

Ning XL, Tan P, Huang DY, Zhou FL (2009), "Application of Adaptive Fuzzy Sliding Mode Control to a Seismically Excited Highway Bridge," *Structural Control and Health Monitoring*, **16**(6): 639–656. https://doi.org/10.1002/stc.324

Narjabadifam P, Hoseinpour R, Noori M and Altabey WA (2021), "Practical Seismic Resilience Evaluation and Crisis Management Planning Through GIS-Based Vulnerability Assessment of Buildings," *Earthquake Engineering and Engineering Vibration*, **20**(1): 25–37. https://doi.org/10.1007/s11803-021-2003-1

Noori M, Wang H, Altabey W A, Silik A I H (2018), "A Modified Wavelet Energy Rate Based Damage Identification Method for Steel Bridges," *Scientia Iranica, International Journal of Science and Technology, Transactions on Mechanical Engineering* (*B*), **25**(6): 3210–3230. https://doi.org/10.24200/sci.2018.20736

Pourzeynali S, Salimi S, Yousefisefat M, Kalesar H E (2016), "Robust Multi-Objective Optimization of STMD Device to Mitigate Buildings Vibrations," *Earthquakes and Structures*, **11**(2): 347–369. https://doi.org/10.1016/j.scient.2012.11.015

Šabanovic A (2011), "Variable Structure Systems with Sliding Modes in Motion Control—A Survey," *IEEE Transactions on Industrial Informatics*, **7**(2): 212–223. https://doi.org/10.1109/TII.2011.2123907

Shtessel Y, Edwards C, Fridman L and Levant A (2014), *Sliding Mode Control and Observation*, Birkhäuser, New York, NY. https://doi.org/10.1007/978-0-8176-4893-0

Shin DK, Phu DX, Choi SM and Choi SB (2016), "An

Adaptive Fuzzy Sliding Mode Control of Magneto-Rheological Seat Suspension with Human Body Model," Intelligent *Material Systems and Structures*, **27**(7): 925–934. https://doi.org/10.1177/1045389X15610902

Silik AI, Noori M, Altabey WA and GhiasiR (2021a), "Comparative Analysis of Wavelet Transform for Time-Frequency Analysis and Transient Localization in Structural Health Monitoring," *Structural Durability & Health Monitoring*, **15**(1): 1–22. https://doi.org/10.32604/sdhm.2021.012751

Silik AI, Noori M, Altabey WA and Ghiasi R (2021b), "Selecting Optimum Levels of Wavelet Multi-Resolution Analysis for Time-Varying Signals in Structural Health Monitoring," *Structural Control and Health Monitoring*. https://doi.org/10.1002/stc.2762 (in Press)

Silik AI, Noori M, Altabey WA, Dang J, Ghiasi R and Wu Z (2021c), "Optimum Wavelet Selection for Nonparametric Analysis Toward Structural Health Monitoring for Processing Big Data from Sensor Network: A Comparative Study," *Structural Health Monitoring*. https://doi.org/10.1177/14759217211010261 (in Press)

Silik AI, Noori M, Altabey WA, Ghiasi R and Wu Z (2021d), "Analytic Wavelet Selection for Time–Frequency Analysis of Big Data Form Civil Structure Monitoring," Chapter 29, *Civil Structural Health Monitoring, Proceedings of CSHM-8 Workshop 2021*, Rainieri C, Fabbrocino G, Caterino N, *et al*. (Eds.), Springer. https://doi.org/10.1007/978-3-030-74258-4_29

Slotine JJ and Li W (1991), *Applied Nonlinear Control*, Prentice Hall: Englewood Cliffs, NJ.

Tangjitsitcharoen S, Saksri T and Ratanakuakangwan S (2015), "Advance in Chatter Detection in Ball End Milling Process by Utilizing Wavelet Transform," *Intelligent Manufacturing*, **26**(3): 485–499. https://doi.org/10.1007/s10845-013-0805-3

Tokat S, Fadali MS and Eray O (2015), "A Classification and Overview of Sliding Mode Controller Sliding Surface Design Methods," *Recent Advances in Sliding Modes: from Control to Intelligent Mechatronics,* Springer, Cham: 417–439. https://doi.org/10.1007/978-3-319-18290-2_20.

Wang AP and Lee CD (2002), "Fuzzy Sliding Mode Control for a Building Structure Based on Genetic Algorithms," *Earthquake Engineering and Structural Dynamics*, **31**(4): 881–895. https://doi.org/10.1002/eqe.127

Wang L and Liang M (2009), "Chatter Detection Based on Probability Distribution of Wavelet Modulus Maxima," *Robotics and Computer-Integrated Manufacturing*, **25**(6): 989–998. https://doi.org/10.1016/j.rcim.2009.04.011

Wang SG (2003), "Robust Active Control for Uncertain Structural Systems with Acceleration Sensors," *Structural Control*, **10**(1): 59–76. https://doi.org/10.1002/stc.17

Wang SG, Roschke PN and Yeh HY (2004), "Robust Control for Structural Systems with Unstructured Uncertainties," *Engineering Mechanics*, **130**(3): 337–346. https://doi.org/10.1061/(ASCE)0733-9399(2004)130:3(337)

Wang T, Altabey WA, Noori M and Ghiasi R (2020a), "A Deep Learning Based Approach for Response Prediction of Beam-Like Structures," *Structural Durability & Health Monitoring*, **14**(4): 315–338. https://doi.org/10.32604/sdhm.2020.011083

Wang T, Noori M and Altabey WA (2020b), "Identification of Cracks in an Euler-Bernoulli Beam Using Bayesian Inference and Closed-Form Solution of Vibration Modes," *Proceedings of the Institution of Mechanical Engineers, Part L: Journal of Materials: Design and Applications*, **235**(2): 421–438. https://doi.org/10.1177/1464420720969719

Wang T, Noori M, Altabey WA, Farrokh M and Ghiasi R (2021), "Parameter Identification and Dynamic Response Analysis of a Modified Prandtl-Ishlinskii Asymmetric Hysteresis Model via Least-Mean Square algorithm and Particle Swarm Optimization," *Proceedings of the Institution of Mechanical Engineers*, *Part L: Journal of Materials: Design and Applications*. https://doi.org/10.1177/14644207211006840 (in Press)

Yang JN, Wu JC, Agrawal AK and Hsu SY (1997) "Sliding Mode Control with Compensator for Wind and Seismic Response Control," *Earthquake Engineering and Structural Dynamics*, **26**(11): 1137–1156.

Yang JN, Wu JC, Reinhorn AM and Riley M (1996) "Control of Sliding-Isolated Buildings Using Sliding-Mode Control," *Structural Engineering*, **122**(2): 179–186. https://doi.org/10.1061/(ASCE)0733-9445

Yao Z, Mei D and Chen Z (2010), "On-Line Chatter Detection and Identification Based on Wavelet and Support Vector Machine," *Materials Processing Technology*, **210**(5): 713–719. https://doi.org/10.1016/j.jmatprotec.2009.11.007

Yu X, Man Z and Wu B (1998) "Design of Fuzzy Sliding-Mode Control Systems," *Fuzzy Sets and Systems*, **95**(3): 295–306. https://doi.org/10.1016/S0165-0114(96)00278-3

Zhang Z, Li H, Meng G, Tu X and Cheng C (2016), "Chatter Detection in Milling Process Based on the Energy Entropy of VMD and WPD," *International Journal of Machine Tools and Manufacture*, **108**: 106–112. https://doi.org/10.1016/j.ijmachtools.2016.06.002

Zhao B, Lu X, Wu M and Mei Z (2000), "Sliding Mode Control of Buildings with Base-Isolation Hybrid Protective System," *Earthquake Engineering and Structural Dynamics*, **29**(3): 315–326.

Zhao Y, Noori M and Altabey WA (2017), "Damage Detection for a Beam Under Transient Excitation via Three Different Algorithms," *Structural Engineering and Mechanics*, **64**(6): 803–817. doi:10.12989/sem.2017.64.6.803

Zhao Y, Noori M, Altabey WA and Awad T (2018a),

"A Comparison of Three Different Methods for the Identification of Hysterically Degrading Structures Using BWBN Model," *Frontiers in Built Environment*, **4**(80): 1–19. https://doi.org/10.3389/fbuil.2018.00080

Zhao Y, Noori M, Altabey WA and Ghiasi R (2018b), "Fatigue Damage Identification for Composite Pipeline Systems Using Electrical Capacitance Sensors," *Smart Materials and Structures*, **27**(8): 085023. http://dx.doi.org/10.1088/1361-665x/aacc99

Zhao Y, Noori M, Altabey WA, Ghiasi R and Wu Z (2018c), "Deep Learning-Based Damage, Load and Support Identification for a Composite Pipeline by Extracting Modal Macro Strains from Dynamic Excitations," *Applied Sciences*, **8**(12): 2564. http://dx.doi.org/10.3390/app8122564

Zhao Y, Noori M, Altabey WA and Beheshti-Aval SB (2018d), "Mode Shape-Based Damage Identification for a Reinforced Concrete Beam Using Wavelet Coefficient Differences and Multiresolution Analysis," *Structural Control and Health Monitoring*, **25**(1): 1–41. doi:10.1002/stc.2041

Zinober ASI (1994), *Variable Structure and Lyapunov Control*, Springer, Berlin, Heidelberg. https://doi.org/10.1007/BFb0033675

Nomenclature:

VSC	Variable structure control
SMC	Sliding mode control
ATMD	Active tuned mass damper
ER	Electro-Rheological
FSMC	Fuzzy sliding mode control
DOF	Degree-of-freedom
CWT	Continuous wavelet transform
2-D CWT	2-D continuous wavelet transform
CL	Control Law
$\boldsymbol{M}, \boldsymbol{C}, \boldsymbol{K}$	Mass, damping and stiffness matrices, respectively
$k_1, k_2, \cdots, k_n$	Stiffness coefficients
$c_1, c_2, \cdots, c_n$	Damping coefficients
$K_t(t)$ and $K_b(t)$	Stiffness coefficients are functions of the dynamic responses
$c_t(t)$ and $c_b(t)$	Damping coefficient are functions of the dynamic responses
$\boldsymbol{P}$	Location matrix of control force
$\boldsymbol{Q}$	Location matrix of external loads
$\boldsymbol{u}(t)$	A vector of control forces
$\boldsymbol{w}(t)$	A vector of external environmental loads or disturbances
$\boldsymbol{z}(t)$	A state vector
$\boldsymbol{A}$	A system matrix
$\boldsymbol{B}$	A control matrix
$\boldsymbol{E}$	A disturbance matrix
$\boldsymbol{R}$	A sliding matrix
η, g, α	Parameters used in the design of control laws
$\mathbb{R}, \mathbb{R}^+$	Real set, positive real set
$L^2(\mathbb{R})$	Two-dimensional set of real integers
ψ	Continuous wavelet function in the time domain
$\overline{\psi}$	Conjugate function
$\boldsymbol{r}_\theta$	2-D rotation matrix